Contents lists available at ScienceDirect

Remote Sensing of Environment

journal homepage: http://ees.elsevier.com

Hybrid inversion of radiative transfer models based on high spatial resolution satellite reflectance data improves fractional vegetation cover retrieval in heterogeneous ecological systems after fire

José Manuel Fernández-Guisuraga [a,*], Jochem Verrelst [c], Leonor Calvo [a], Susana Suárez-Seoane [b]

[a] Area of Ecology, Faculty of Biological and Environmental Sciences, University of León, 24071 León, Spain
[b] Department of Organisms and Systems Biology (Ecology Unit) and Research Unit of Biodiversity (UO-CSIC-PA), University of Oviedo, Oviedo, Mieres, Spain
[c] Image Processing Laboratory (IPL), Parc Científic, University of Valencia, 46980 Paterna, Valencia, Spain

ARTICLE INFO

Keywords
Forest fire
Fractional vegetation cover
Radiative transfer modeling
Sentinel-2
WorldView-3

ABSTRACT

In forest landscapes affected by fire, the estimation of fractional vegetation cover (FVC) from remote sensing data using radiative transfer models (RTMs) enables to evaluate the ecological impact of such disturbance across plant communities at different spatio-temporal scales. Even though, when landscapes are highly heterogeneous, the fine-scale ground spatial variation might not be properly captured if FVC products are provided at moderate or coarse spatial scales, as typical of most of operational Earth observing satellite missions. The objective of this study was to evaluate the potential of a RTM inversion approach for estimating FVC from satellite reflectance data at high spatial resolution as compared to the standard use of coarser imagery. The study was conducted both at landscape and plant community levels within the perimeter of a megafire that occurred in western Mediterranean Basin. We developed a hybrid retrieval scheme based on PROSAIL-D RTM simulations to create a training dataset of top-of-canopy spectral reflectance and the corresponding FVC for the dominant plant communities. The machine learning algorithm Gaussian Processes Regression (GPR) was learned on the training dataset to model the relationship between canopy reflectance and FVC. The GPR model was then applied to retrieve FVC from WorldView-3 (spatial resolution of 2 m) and Sentinel-2 (spatial resolution of 20 m) surface reflectance bands. A set of 75 plots of 2x2m and 45 plots of 20x20m was distributed under a stratified schema across the focal plant communities within the fire perimeter to validate FVC satellite derived retrieval. At landscape scale, the accuracy of the FVC retrieval was substantially higher from WorldView-3 (R^2 = 0.83; RMSE = 7.92%) than from Sentinel-2 (R^2 = 0.73; RMSE = 11.89%). At community level, FVC retrieval was more accurate for oak forests than for heathlands and broomlands. The retrieval from WorldView-3 minimized the over- and underestimation effects at low and high field sampled vegetation cover, respectively. These findings emphasize the effectiveness of high spatial resolution satellite reflectance data to capture FVC ground spatial variability in heterogeneous burned areas using a hybrid RTM retrieval method.

1. Introduction

Wildfires are major ecological disturbances across most terrestrial ecosystems around the globe (De Santis and Chuvieco, 2007; Bennett et al., 2016; Collins et al., 2018), causing significant impacts on their biological composition, structure and functioning (Calvo et al., 2008; Lozano et al., 2008) and, therefore, on the ecosystem capacity to provide services and goods for society (Lee et al., 2015; Robinne et al., 2020). The fire-induced shifts in ecosystem structure and composition further influence land surface energy budgets at local, regional and continental scales over a long time period after fire (Liu et al., 2005; Archibald et al., 2018) by changes on earth surface albedo (Kasischke and Stocks, 2000), as well as sensible and latent heat flux (Liu et al., 2018), among others. In the European Mediterranean Basin, the frequency of large and severe forest fires has increased to a great extent in the recent decades (Pausas et al., 2008; González-De Vega et al., 2016) as a consequence of land-use changes (Chergui et al., 2018), socio-economic factors, such as rural depopulation, abandonment of the primary sector or tourism pressure (Pausas and Keeley, 2014; Chergui et al., 2018), and climate change (González-De Vega et al., 2016). In this context, the assessment of vegetation structure variation across the landscape is essential to determine the impact of fire on vegetation communities in the short or medium term at different spatial scales (Veraverbeke et al., 2012a; Fernández-Guisuraga et al., 2020) and, therefore, to address sustainable management actions on high-priority areas aimed to avoid the most harmful environmental fire effects (De Santis et al., 2009).

Fractional vegetation cover (FVC) is a crucial biophysical property to be considered in post-fire environmental assessments, as it enables to quantify the vegetation horizontal structure across landscapes (Chu et al., 2016; Fernández-Guisuraga et al., 2020). FVC is defined as the ratio of green vegetation vertical projected area to the considered land surface extension (Gutman and Ignatov, 1998; Gitelson et al., 2002; Jia et al., 2016; Song et al., 2017; García-Haro et al., 2018). This parameter has been demon-

* Corresponding author.
E-mail address: jofeg@unileon.es (J.M. Fernández-Guisuraga)

strated to be particularly useful for determining forest response and resilience to fire disturbance (Fernández-Guisuraga et al., 2019a), characterizing fuel loadings in fire-prone ecosystems (Suchar and Crookston, 2010; Wing et al., 2012), as well as for identifying sensitive areas to soil erosion or nutrient losses as a result of changes in vegetation cover, and, therefore, in hydrogeological processes (Veraverbeke et al., 2012b; Chu et al., 2016; Storey et al., 2016; Fernández-Guisuraga et al., 2020). Thus, post-fire FVC assessment of vegetation legacies is of significant meaning for restoring fire-disturbed vegetation communities, particularly those affected by high burn severity events in fire-prone ecosystems (Quayle et al., 2005; Kokaly et al., 2007) and refining fire behavior models in case of the occurrence of a new wildfire (Wing et al., 2012; Fernández-Guisuraga et al., 2019a). Additionally, FVC monitoring allows to elucidate relationships between fire disturbances and energy balance processes such as evapotranspiration (Weiss et al., 2000; Song et al., 2017), as well as land surface albedo and emissivity (Zhou et al., 2007). Although ground surveys provide the most accurate FVC measures through visual estimations or instrumental methods (Zhang et al., 2013; Li et al., 2015a), this approach is expensive and labor-intensive (Liang et al., 2008; Fernández-Guisuraga et al., 2020), which makes it unfeasible for monitoring large burned landscapes (Chuvieco and Kasischke, 2007; Fernández-Guisuraga et al., 2019a). Currently, the most feasible alternative to estimate FVC in extensive areas, as compared to traditional field sampling campaigns, is the use of remote sensing techniques (Veraverbeke et al., 2012a; Jia et al., 2016; Fernández-Guisuraga et al., 2020) in combination with FVC field measurements for validation (White et al., 2000). The most commonly used algorithms to estimate FVC from remote sensing data include: (i) empirical models based on the establishment of statistical relationships between field-measured FVC and reflectance data or its derived products, such as spectral indices or texture metrics (e.g. Los et al., 2000; Gitelson et al., 2002; Goetz et al., 2006; Cuevas-González et al., 2009; Jiapaer et al., 2011; Hill et al., 2017; Fernández-Guisuraga et al., 2019a; Fernández-Guisuraga et al., 2019b); (ii) pixel unmixing models, which assume that remote sensing pixel spectra is a combination of two or more ground components, being the vegetation component the pixel FVC (e.g. Gutman and Ignatov, 1998; Xiao and Moody, 2005; Jiapaer et al., 2011; Veraverbeke et al., 2012a; Zhang et al., 2013; Li et al., 2015a; Bian et al., 2016; Fernández-Guisuraga et al., 2020); and (iii) physical-based methods based on the inversion of radiative transfer models (RTM) (e.g. Baret et al., 2007; Kallel et al., 2007; Ding et al., 2016; Jia et al., 2016; García-Haro et al., 2018; Wang et al., 2017; Wang et al., 2018; Tao et al., 2019).

Among these approaches, the inversion of radiative transfer models (RTMs) to retrieve FVC is the method with the soundest theoretical basis and physical sense (Jia et al., 2015; Verrelst et al., 2015a). RTMs simulate the physical relationships between canopy reflectance and vegetation biophysical variables (Jia et al., 2016; Wang et al., 2017) and can be inverted using observed reflectance data to retrieve FVC. The RTM physical relationships are independent of ecosystem environmental conditions (Yebra et al., 2008; Yebra and Chuvieco, 2009) and, therefore, the models are widely applicable over large areas with heterogeneous ground cover (Tao et al., 2019). RTM parametrization is usually based on field knowledge or measurements for a specific plant community (Campos-Taberner et al., 2018). However, when aiming to encompass a wide range of communities for which no ground data is available, then the model variables are ranged between specific thresholds (Yebra and Chuvieco, 2009). A wide range of coupled leaf and canopy RTM models have been used in the recent years to retrieve vegetation biophysical parameters such as FVC (e.g. DART, Gastellu-Etchegorry et al., 2004; INFORM, Schlerf and Atzberger, 2006; PROSPECT + GeoSail, Verhoef and Bach, 2003; PROSAIL, Jacquemoud et al., 2009). In particular, PROSAIL has been one of the most frequently applied models over the past years for simulating canopy spectra and retrieving vegetation biophysical parameters, even in the case of heterogeneous canopies (Yebra and Chuvieco, 2009; Verrelst et al., 2015a; García-Haro et al., 2018; Lin et al., 2019) due to its robustness, accuracy and computational efficiency (Jacquemoud et al., 2009). However, the direct inversion cedure (Yebra et al., 2008; Verrelst et al., 2015a). Therefore, indirect RTM inversion is typically performed through either lookup-tables (LUT) (physical inversion) or machine learning regression algorithms (MLRA) (hybrid inversion) strategies (Verger et al., 2011; Jia et al., 2016; Campos-Taberner et al., 2018). Among them, MLRA hybrid inversion ensures: (i) a high degree of model generalization (Houborg and McCabe, 2018), (ii) more accurate biophysical parameter estimation (Verger et al., 2011; Liang et al., 2015) and (iii) better computational efficiency (Yang et al., 2016; García-Haro et al., 2018) than other retrieval strategies.

Conventionally, MLRA trained over RTM simulations have been used to retrieve FVC from data collected by operational satellite optical sensors with low spatial resolution (e.g. MODIS, MetOp-AVHRR, MERIS, SPOT-VEGETATION) (Bacour et al., 2006; Baret et al., 2007; Jia et al., 2015; Yang et al., 2016; Campos-Taberner et al., 2018; García-Haro et al., 2018) or moderate spatial resolution (e.g. Landsat, CHRIS/PROBA, Sentinel-2, GF-1 WFV) (Verger et al., 2011; Li et al., 2015b; Jia et al., 2016; Yang et al., 2017a; Wang et al., 2018; Upreti et al., 2019; Hu et al., 2020) at local, regional or global scales. Nevertheless, the fine-scale ground spatial variation of heterogeneous post-fire landscapes generated by complex mixtures of plant communities, soil types and fine or coarse charred woody debris (Fernández-Guisuraga et al., 2020) might not be properly captured at the spatial scale of the aforementioned FVC products (Sinha et al., 2020). In such cases, high spatial resolution satellite data are needed to: (i) Account for the fine-grained arrangement in small patches of living vegetation legacies (Lentile et al., 2006; Walker et al., 2019). These patches play a key role in post-fire vegetation recovery, as they might act as seed sources and dispersers habitat (Schlawin and Zahawi, 2008), as well as a controllers of the runoff erosive power (Puigdefábregas, 2005). Consequently, their omission will result in the underestimation of vegetation natural regeneration capacity and soil protection against erosion (Ludwig et al., 2005; Walker et al., 2019). (ii) Detect mortality at individual tree level (Lentile et al., 2006), which is essential in post-fire management strategies. (iii) Obtain operational FVC maps, at scales of at least 1:10,000, which allow the identification of high-priority areas where emergency management actions are necessary at short term for assisting vegetation recovery and controlling soil erosion processes (Corona et al., 2008). (iv) Assess post-fire vegetation dynamics at medium or long term to monitor ecosystem resilience at high temporal resolution (i.e. low revisit time) (Van Leeuwen, 2008; Veraverbeke et al., 2011). Traditionally, coarse spatial resolution satellite optical sensors with high temporal frequency (e.g. MODIS) have been used to monitor post-fire vegetation dynamics (Van Leeuwen, 2008). However, the current availability of moderate or high spatial resolution sensors with low revisit times (e.g. Sensinel-2 and commercial satellites such as Deimos-2 or WorldView-3) provides a great opportunity for monitoring vegetation condition in post-fire landscapes.

Remote sensing data at high spatial resolution have received little attention in the fire ecology field for post-fire FVC analysis (Fernández-Guisuraga et al., 2020). Despite all the available knowledge on this topic, there is still a gap in estimating FVC from the inversion of an RTM using satellite reflectance data at high spatial resolution. This fact is particularly relevant in complex and heterogeneous burned landscapes made of a mixture of different shrub and tree communities, bare soil and woody debris. The objective of this study was therefore to evaluate the potential of a hybrid RTM inversion approach for estimating FVC from satellite reflectance data at high spatial resolution, as compared to the standard use of coarser imagery. The case study was conducted in a heterogeneous burned landscape of the western Mediterranean Basin that comprises different shrubland and tree forest communities. Specifically, we analyzed the performance of WorldView-3 (spatial resolution of 2 m) and Sentinel-2 (spatial resolution of 20 m) surface reflectance data to retrieve FVC at landscape and plant community levels using Gaussian processes regression (GPR) algorithm learned from a simulation dataset generated using the PROSAIL-D model. We seek to address the following research questions:

(i) Do remote sensing data at high spatial resolution provide quanti-

(ii) Does a hybrid RTM retrieval method to estimate FVC provide an accuracy above the accepted threshold of 10% for vegetation biophysical variable retrieval (Drusch et al., 2012; Verrelst et al., 2016) in heterogeneous post-fire environments generated by complex mixtures of vegetation and soil types, as well as charred woody legacies?

2. Material and methods

2.1. Study site

The study area is located within the perimeter of a mixed-severity wildfire (Sierra de Cabrera mountain range, NW Spain; Fig. 1) that burned 9940 ha between 21th and 27th August 2017. It lays at the limit of the Mediterranean and Eurosiberian biogeographic regions (Rivas-Martínez et al., 2011). Altitude ranges between 834 and 1963 m a.s.l. and orography is abrupt. The climate is Mediterranean temperate (García-Llamas et al., 2019), with an average annual temperature of 9 °C and an average annual precipitation of 850 mm (Ninyerola et al., 2005). Soils are predominantly acidic and developed over siliceous lithologies (slates in the north of the fire perimeter and quartzite in the south area), mainly Lithic and Distric Leptosols (LPq and LPd, respectively) and Distric and Humic Cambisols (CMd and CMu, respectively) (GEODE, 2019; ITACyL, 2019). The burned landscape is highly heterogeneous since it holds a wide range of plant communities: shrublands dominated by *Genista hystrix* Lange, *Erica australis* L. and *Genista florida* L. and forests dominated by *Quercus pyrenaica* Willd. and *Pinus sylvestris* L. Each community exhibits also high levels of ground spatial heterogeneity due to local differences in post-fire regeneration patterns, accumulation of non-photosynthetic material and bare soil (Fernández-Guisuraga et al., unpublished).

Fire has been historically a crucial process modeling the landscape dynamics of the study site, the fire regime being characterized by a high wildfire frequency (8.48 fires × 10 years^{-1}) (García-Llamas et al., 2020) and severity (García-Llamas et al., 2019). In fact, the adaptive traits (e.g. vegetative resprouting, heat-shock triggered germination or self-pruning) of the dominant plant species are typical of fire-prone landscapes (Keeley and Zedler, 1998; Calvo et al., 2008; Fernandes et al., 2008).

2.2. Satellite imagery data and pre-processing

Sentinel-2 multispectral imaging mission comprises two polar-orbiting satellites placed in the same sun-synchronous orbit, launched on 23rd June 2015 (Sentinel-2A) and 7th March 2017 (Sentinel-2B) as part of the Copernicus program of the European Space Agency (ESA, 2020). Sentinel-2 provides 13 spectral bands -four bands at 10 m, six bands at 20 m and three bands at 60 m of spatial resolution- over the visible (VIS), near infrared (NIR) and shortwave infrared (SWIR) regions of the spectrum (Table 1). Sentinel-2 MSI Level 1C (top-of-atmosphere reflectance) scene covering the study site was acquired from the Copernicus Open Access Hub on 23rd August 2019 at 11:21:21 with a cloud cover of 1.38%. Sentinel-2 MSI Level 1C scene was already orthorectified by the image provider. The bands at 10 m of spatial resolution were resampled to 20 m using a nearest neighbor technique. The pre-processing included topographic and atmospheric correction to obtain a surface reflectance product (Level 2A) using the ATCOR algorithm (Richter and Schläpfer,

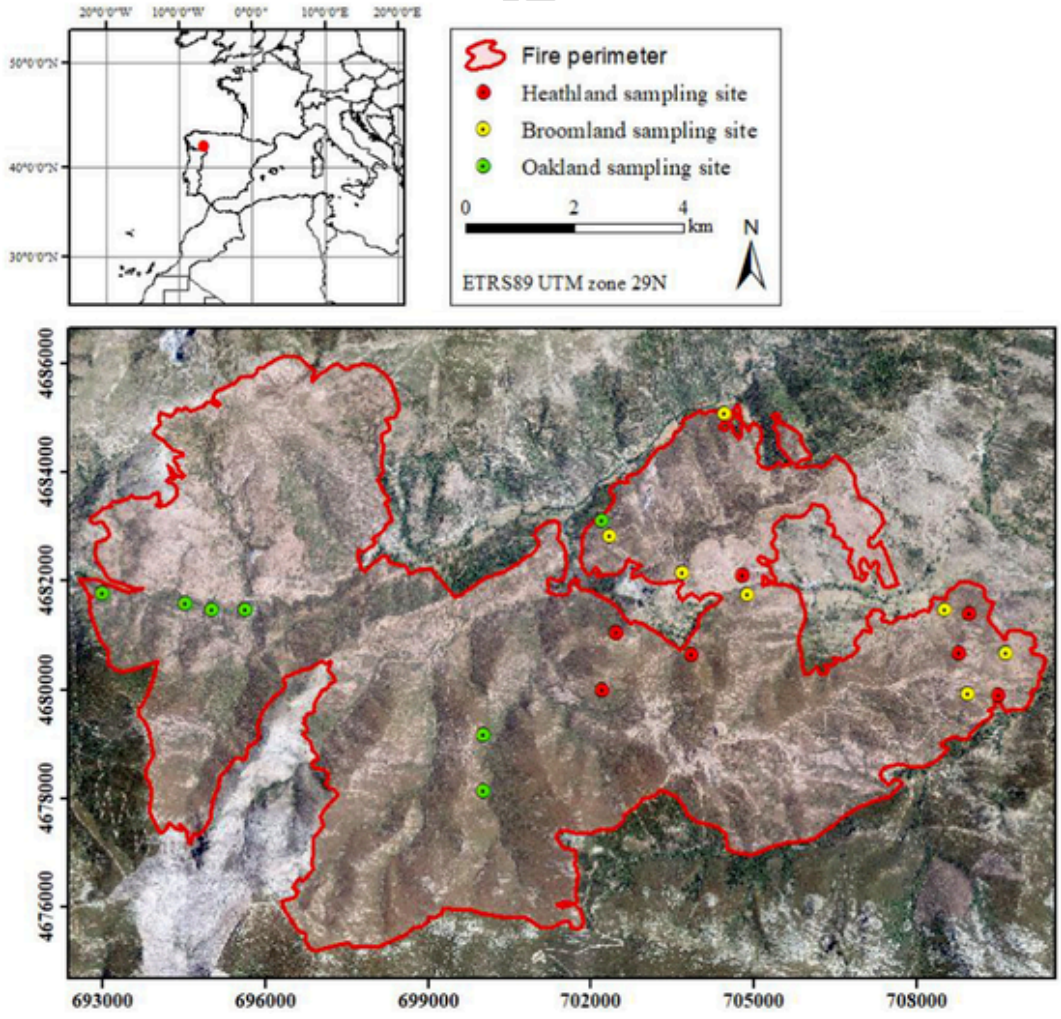

Fig. 1. Sierra de Cabrera wildfire (NW Spain) occurred in August 2017 and location of the sampling sites for each studied plant community (heathlands, broomlands and oak forests).

Table 1
WorldView-3 and Sentinel-2 band configuration. Those considered for further analysis are bolded.

WorldView-3	B1	**B2**	**B3**	B4	**B5**	**B6**	**B7**	B8	B9	**B10**	B11	B12	B13	**B14**	B15	B16
Spatial resolution (m)	1.2	**1.2**	**1.2**	1.2	**1.2**	**1.2**	**1.2**	1.2	3.7	**3.7**	3.7	3.7	3.7	**3.7**	3.7	3.7
Band center (nm)	425	**480**	**545**	605	**660**	**725**	**833**	950	1210	**1570**	1660	1730	2165	**2205**	2260	2330
Band width (nm)	50	**60**	**70**	40	**60**	**40**	**125**	180	30	**40**	40	40	40	**40**	50	70
Sentinel-2A	B1	**B2**	**B3**	**B4**	B5	**B6**	B7	**B8**	B8A	B9	B10	**B11**	**B12**			
Spatial resolution (m)	60	**10**	**10**	**10**	20	**20**	20	**10**	20	60	60	**20**	**20**			
Band center (nm)	443	**492**	**560**	**665**	704	**741**	783	**833**	865	945	1374	**1614**	**2202**			
Band width (nm)	21	**66**	**36**	**31**	15	**15**	20	**106**	21	20	31	**91**	**175**			

2018) bundled in PCI Geomatica 2018 software (PCI Geomatics Enterprises Inc.).

WorldView-3 is a polar sun-synchronous commercial satellite launched on 13th August 2014 (DigitalGlobe, 2020). Sensors on-board WorldView-3 provide 16 spectral bands, featuring eight bands over the VIS and NIR regions at 1.24 m of spatial resolution and eight bands over the SWIR region with a spatial resolution of 3.7 m (Table 1). VIS and NIR bands were resampled to 2 m by the image provider and SWIR bands were released commercially at 7.5 m of spatial resolution (Asadzadeh and de Souza-Filho, 2016). WorldView-3 scene was acquired on 22nd August 2019 at 11:38:57 with absence of cloud cover. SWIR bands were resampled to 2 m using a nearest neighbor technique. The scene was orthorectified using the rational polynomial coefficients provided in the image metadata and a Digital Elevation Model (DEM) at 5 m of spatial resolution with an $RMSE_Z$ (vertical accuracy) < 20 cm provided by the Spanish National Center of Geographic Information (http://www.cnig.es/). Image pre-processing was similar to that applied to Sentinel-2 MSI Level 1C scene.

WorldView-3 and Sentinel-2 common bands with similar band center and width (Table 1 and Fig. 2) were considered for further analyses after discarding WorldView-3 band 1 and Sentinel-2 bands 1, 9 and 10 at 60 m. These bands are used for atmospheric correction and cloud detection (Wang et al., 2018) and they are influenced by atmospheric effects (Jia et al., 2016). For that reason, these bands cannot provide top of canopy reflectances interpretable by RTMs (Rivera et al., 2013).

See Figure SM2 of the Supplementary material for a RGB view of WorldView-3 and Sentinel-2 imagery covering the perimeter of the Sierra de Cabrera wildfire.

2.3. FVC estimation using machine learning inversion of radiative transfer model (RTM)

PROSAIL-D RTM (the coupled PROSPECT-D leaf optical model and SAIL canopy reflectance model) was used in this study in forward mode to create a training dataset of top of canopy spectral reflectance from 400 to 2500 nm and the corresponding FVC under several canopy conditions. The dataset was spectrally resampled to simulate WorldView-3 and Sentinel-2 satellite observations of canopy reflectance. A Gaussian processes regression (GPR) algorithm was learned on the training dataset to model the relationship between the simulated reflectance and FVC. The model was then used to retrieve FVC from the WorldView-3 and Sentinel-2 surface reflectance values (Fig. 3). These analyses were conducted within ARTMO (Automated Radiative Transfer Models Operator) software package (Verrelst et al., 2012a).

2.3.1. Canopy reflectance simulation

The PROSAIL model (Jacquemoud et al., 2009), which results from the coupling of PROSPECT (Jacquemoud and Baret, 1990) and SAIL (Verhoef, 1984; Verhoef, 1985) RTMs, was used to produce top of canopy spectral reflectance simulations.

In PROSPECT, leaf directional-hemispherical reflectance and transmittance are simulated for the optical spectrum from 400 to 2500 nm with a 1 nm spectral resolution (Jacquemoud and Baret, 1990; Verrelst et al., 2015a) as a

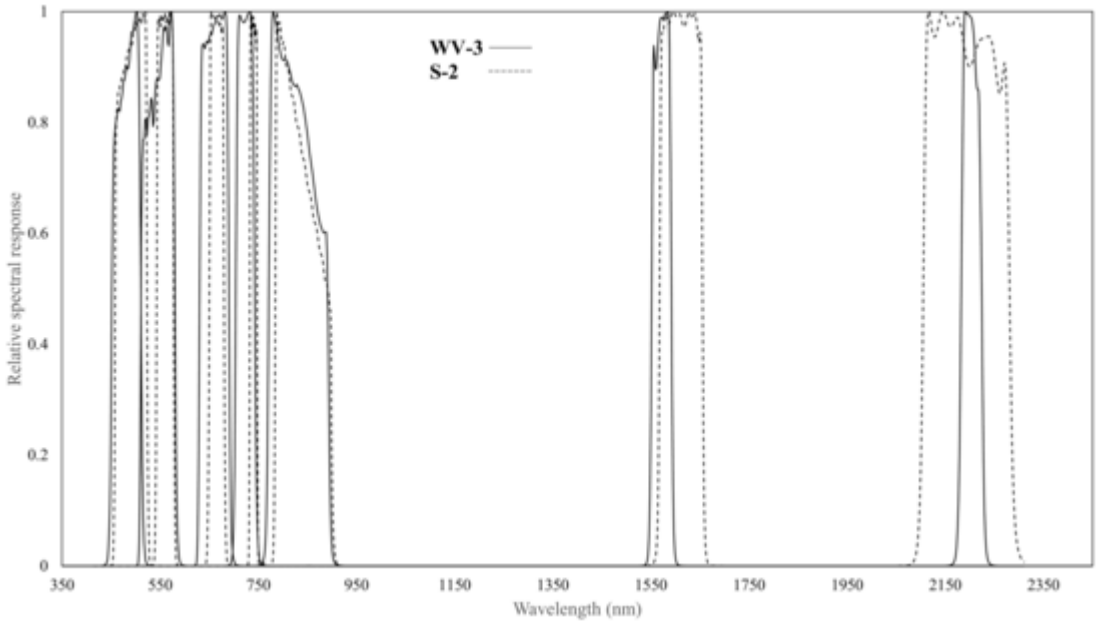

Fig. 2. Spectral Response for the WorldView-3 (WV-3) and Sentinel-2 (S-2) bands.

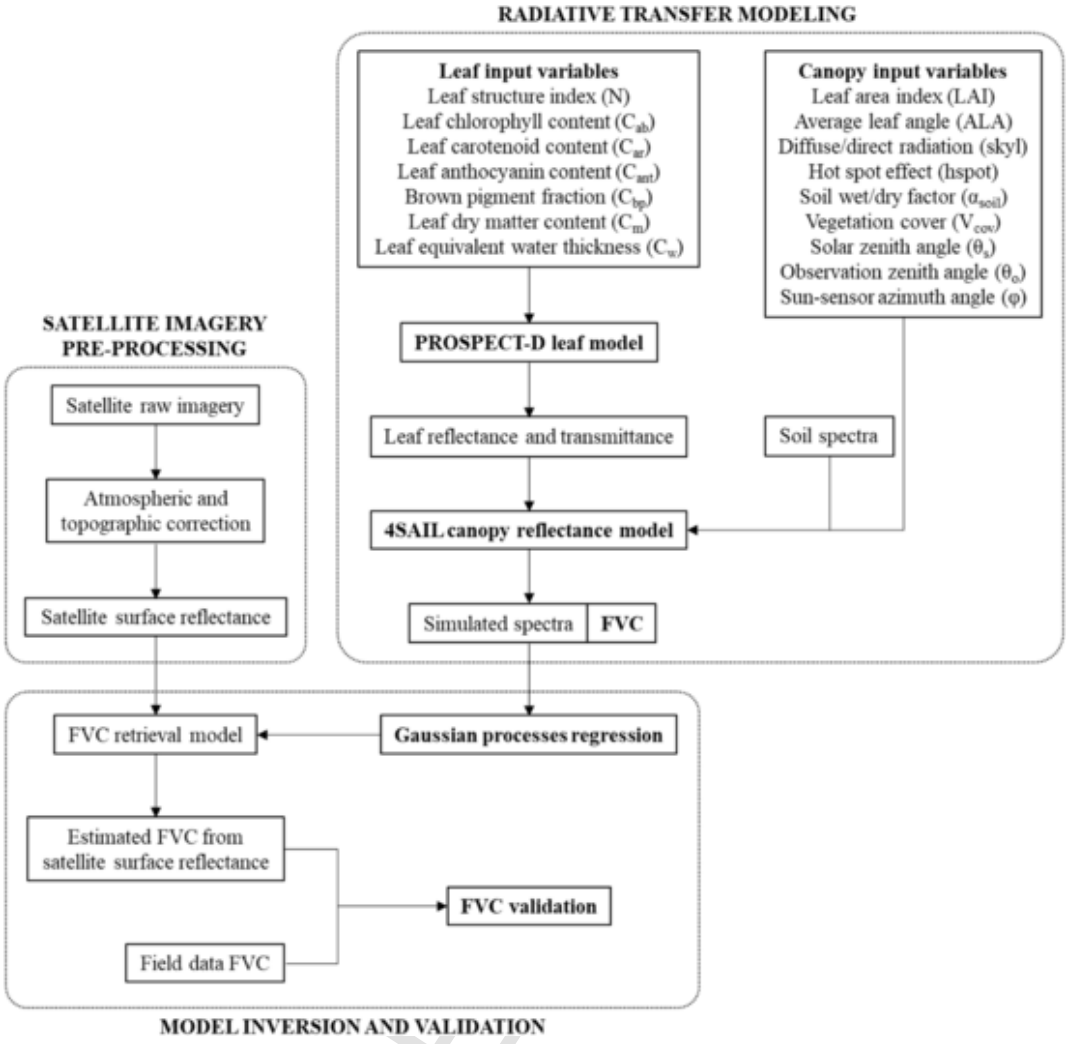

Fig. 3. Flowchart of radiative transfer model (RTM) inversion and validation.

function of leaf structure parameter (N) and several biochemical variables (Casas et al., 2014). For the model version used in this study (PROSPECT-D; Féret et al., 2017), the required biochemical variables are: leaf chlorophyll content (C_{ab}), leaf carotenoid content (C_{ar}), leaf anthocyanin content (C_{ant}), brown pigment fraction (C_{bp}), leaf dry matter content (C_m) and leaf equivalent water thickness (C_w). We have chosen this version since it adds anthocyanins to chlorophylls and carotenoids to the previous version of the model (PROSPECT-5) and improves model performance with or without the presence of the new pigment in the vegetation (Féret et al., 2017). In our study, the inclusion of anthocyanins in the model provides a substantial added value, since these pigments are essential leaf constituents that play a significant role in the vegetation leaf optical signal under environmental stress conditions (Gould, 2004), such after the occurrence of a wildfire (Fernández-Guisuraga et al., 2019a). The ranges of the PROSPECT-D input variables (Table 2) related to pigments content were established on the basis of literature review and expert field knowledge to account for the variability of the plant communities of the study site (Baret et al., 2007; Féret et al., 2017; Campos-Taberner et al., 2018; Wang et al., 2018; Tao et al., 2019). Despite brown pigment fraction (C_{bp}) is removed or fixed to zero in some studies (e.g. Jay et al., 2016; Campos-Taberner et al., 2018; García-Haro et al., 2018), we used it due to its large influence in the red edge region of the vegetation spectrum. Brown pigments are not always related to visible leaf browning, but with chlorophyll breakdown in senescent stages (Danner et al., 2019). Leaf structure variable (N) was allowed to range between 1.5 and 2.5, a suitable range for dicotyledons

Table 2
Range of input variables of the PROSPECT-D and 4SAIL models.

	Unit	Range or value
Leaf parameters (PROSPECT-D)		
Leaf structure index (N)	–	1.5–2.5
Leaf chlorophyll content (C_{ab})	$\mu g\ cm^{-2}$	20–90
Leaf carotenoid content (C_{ar})	$\mu g\ cm^{-2}$	5–40
Leaf anthocyanin content (C_{ant})	$\mu g\ cm^{-2}$	0–40
Leaf dry matter content (C_m)	$g\ cm^{-2}$	0.005–0.015
Leaf equivalent water thickness (C_w)	$g\ cm^{-2}$	0.005–0.015
Brown pigment fraction (C_{bp})	–	0–1
Canopy parameters (4SAIL)		
Leaf area index (LAI)	$m^2\ m^{-2}$	0.1–6
Average leaf angle (ALA)	°	30–80
Diffuse/direct radiation (skyl)	–	0.1
Hot spot effect (hspot)	–	0.001–1
Soil brightness factor (α_{soil})	–	0–1
Vegetation cover (V_{cov})	–	0–1
Solar zenith angle (θ_s)	°	32.2
Observation zenith angle (θ_o)	°	19.1
Sun-sensor azimuth angle (φ)	°	42.6

(Sinha et al., 2020). A uniform distribution was assumed for each PROSPECT-D variable.

Leaf reflectance and transmittance simulated by PROSPECT-D serves as input for SAIL, a 1-D turbid medium canopy reflectance model (Jacquemoud et al., 2009), which assumes a random distribution of leaves (Baret et al., 2007). We used an improved version of the model -4SAIL- developed by Verhoef et al. (2007), which is more numerically robust and stable than previous SAIL models (Jacquemoud et al., 2006) and requires as input variables: leaf area index (LAI), average leaf angle (ALA), ratio between diffuse and direct radiation (skyl), hot spot effect (hspot) specified as the ratio between leaves size and canopy height (Casas et al., 2014), soil background reflectance, soil brightness factor (α_{soil}) and viewing geometry (solar zenith angle -θ_s-, observation zenith angle -θ_o- and sun-sensor azimuth angle -φ-). LAI, ALA, skyl and hspot input variables were established in agreement with the literature and field knowledge to consider the complete ground cover variability of the study site (Baret et al., 2007; Campos-Taberner et al., 2018) (Table 2). The viewing geometry input variables were fixed from the satellite scene metadata. Soil spectra was extracted from dry and moist bare soil pixels identified in the satellite imagery (Verrelst et al., 2015a) for each prevailing soil type in the study area, multiplied by a soil brightness factor (α_{soil}) scaled between 0 and 1. An accurate soil background reflectance characterization is crucial to produce realistic simulations in ecosystems with sparse canopies (García-Haro et al., 2018). A uniform distribution was also assumed for each 4SAIL input variable.

FVC was computed in PROSAIL-D using gap fraction calculation at nadir (Nilson, 1971) as a function of LAI, ALA and the viewing angle (García-Haro et al., 2018; Wang et al., 2018). Non-vegetated areas at subpixel level must be represented in reflectance simulations of turbid medium RTMs (Campos-Taberner et al., 2016; Svendsen et al., 2018). A linear spectral mixing model was used to account for spatial heterogeneity in the burned landscape (Baret et al., 2007;), which assumes that each pixel is constituted by a linear mixture of pure vegetation fraction (V_{cov}) and bare soil (1-V_{cov}). Then, the simulated reflectance and FVC were computed at the pixel level following this assumption (García-Haro et al., 2018).

Each possible combination of the leaf and canopy input variables listed in Table 2 was used by PROSAIL-D run in forward mode to simulate a training dataset of canopy reflectance from 400 to 2500 nm and the corresponding FVC. We performed a balanced sampling of 2000 simulations over the total model space using Latin Hypercube Sampling (McKay et al., 1979). Additionally, we included a 10% of spectra representative of bare soil ($V_{cov} = 0$) with respect to the total model samples. Likewise, a 10% of spectra corresponding to fine and coarse charred woody debris extracted from the satellite imagery was included to the simulated PROSAIL-D spectra to account for this representative constituent of a burned landscape at short or medium-term. The reflectance simulations were resampled to match the band settings of WorldView-3 and Sentinel-2 using the spectral bandwidth and the relative spectral response of each sensor. A relative white Gaussian noise of 2% wavelength-independent was added to the simulated PROSAIL-D reflectance to account for uncertainties in satellite surface reflectance data derived from the atmospheric correction algorithm, residual cloud contamination and inherent limitations of RTMs (Baret et al., 2007; Jia et al., 2016; García-Haro et al., 2018).

2.3.2. FVC retrieval

The relationship between simulated WorldView-3 and Sentinel-2 reflectance and the corresponding FVC was modeled with Gaussian processes regression (GPR; Rasmussen and Williams, 2006). GPR is a powerful machine learning regression algorithm (MLRA) that has been recently introduced in the field of biophysical parameters estimation (Verrelst et al., 2015b). Gaussian processes provide a Bayesian probabilistic approach for learning regression kernels by fitting non-parametric as well as non-linear models between simulated reflectance data and vegetation biophysical variables (Verrelst et al., 2015b; Sinha et al., 2020), described by a mean and a covariance function (radial basis function kernel) (Verrelst et al., 2012b). GPR offers three meaningful mean FVC prediction and associated uncertainty for the prediction (Verrelst et al., 2012b; Verrelst et al., 2015b; Verrelst et al., 2016). In earlier retrieval studies, GPR slightly outperformed other MLRAs, such as support vector regression (SVR), kernel ridge regression (KRR) or artificial neural networks (ANNs), being computationally more efficient (Verrelst et al., 2012c). See Rasmussen and Williams (2006) for in-depth details of GPR theoretical aspects.

We ran two GPR models for each sensor: (i) a "full model" trained with all bands (Table 1) and (ii) a "parsimonious model" trained with the most contributing bands, according to the theoretical or internal model validation (i.e. with the simulated reflectance data and FVC) based on the model hyperparameter σ_b, which controls the spread of the relations for each band of the simulated reflectance data. The inverse of hyperparameter σ_b represents the importance of band *b*. A high σ_b value indicate that relations extend to a large extent along band *b*, thus suggesting a low band informative content (Verrelst et al., 2012b). This hyperparameter can therefore be exploited to perform a sequential backward band removal (SBBR) routine to identify the set of bands that maximize the predictive performance of the biophysical variable (Verrelst et al., 2016), in this case the FVC. The GPR-SBBR routine was used together with 10-fold cross-validation (10-CV) to identify the most contributing reflectance band subset for FVC prediction applied to the training dataset of PROSAIL-D simulations. We established a hyperparameter σ_b threshold that defines the most informative bands based on the results of 10-CV for both WorldView-3 and Sentinel-2 training datasets. This analysis also allowed to determine if the contribution of the best matching bands for both sensors was similar. The predictive performance of full and parsimonious models was measured by means of root-mean-squared error of cross-validation ($RMSE_{CV}$; i.e. the RMSE average of each cross-validation iteration). FVC was finally retrieved by applying full and parsimonious models to WorldView-3 and Sentinel-2 observed reflectance. An FVC map was generated using the best performing model achieved for each sensor, with mean predictions and their associated uncertainty, since GPR models provide a full posterior predictive distribution (Verrelst et al., 2016).

2.4. Field measurement of FVC and retrieval validation

Two sets of 45 plots equivalent to WorldView-3 and Sentinel-2 pixel size (2 m × 2 m and 20 m × 20 m, respectively) were established in the field between June and July 2019 within the fire perimeter, using each satellite image pixel grid to ensure the alignment between remote sensing and field data. The plots were located using a sub-meter accuracy GPS receiver. The field plots were stratified into the three dominant plant communities across the burned landscape: (i) *Quercus pyrenaica* oakland, (ii) *Erica australis* heathland and (iii) *Genista florida* broomland. FVC was measured in each plot as the vertical projected area occupied by herbs, shrub and tree strata to the total plot extent (Anderson et al., 2005; Calvo et al., 2008; Fernández-Guisuraga et al., 2020) using a visual estimation method in steps of 5% (Schlerf and Atzberger, 2006; Delamater et al., 2012; Liang et al., 2012). FVC was estimated in each plot by four observers, being the final value the average of the four estimations. The standard deviation of the measures taken in each plot was less than 5%. In the 2 m × 2 m plots, FVC was estimated using a quadrat (i.e. a metal frame) of that size. The quadrat was also used in the 20 m × 20 m plots to estimate the FVC in nested sub-plots for reducing subjectiveness. The FVC of each 20 m × 20 m plot was then obtained by averaging the estimation of the sub-plots. In plant communities with several vertical strata, the FVC of the tree canopy was estimated in a bottom-up direction using a quadrat held by long sticks, while a top-down direction was used for estimating the FVC of the understory vegetation (Jia et al., 2016). Thus, the FVC in these communities accounted for the tree canopy plus the understory vegetation which is estimated to be viewed through canopy gaps (Mu et al., 2015). To validate retrieval performance, we computed the coefficient of determination (R^2) and the root-mean-squared error (RMSE) for the relationship between the retrieved FVC from WorldView-3 and Sentinel-2 imagery using the full and parsimonious GPR models, and the field-measured FVC, both at community and landscape (encompassing field data from the three considered communities) levels.

3. Results

The contribution of the most informative bands in the GPR models was approximately identical for WorldView-3 and Sentinel-2 simulated reflectance data, which supports further comparison of the FVC retrieval performance from both datasets. Sharp differences in the band contribution were observed for both sensors across the different spectral regions (Fig. 4A and B). According to theoretical 10-CV, blue and red were the most informative bands throughout the visible region for both sensors, around 420 nm and 660 nm, respectively. The hyperparameter σ_b values were lower than five, which is the highest σ_b value for each selected band in the GPR model that minimizes the RMSEcv in 10-CV, as shown in Fig. 5. Regarding the NIR region, WorldView-3 and Sentinel-2 bands centered at 833 nm soundly contributed (hyperparameter σ_b lower than five) to the GPR model. For the case of the SWIR region, Sentinel-2 and WorldView-3 bands centered around 1600 nm and 2200 nm were highly informative for FVC estimation (hyperparameter σ_b lower than five).

The theoretical validation of the full GPR models trained with all the simulated bands and the corresponding FVC achieved an $RMSE_{cv}$ of 3.36% and 2.97%, respectively for Worldview-3 and Sentinel-2 (Fig. 5A and B). The Worldview-3 parsimonious FVC model, which included the five most contributing bands of the visible, NIR and SWIR regions (Fig. 4A) featured a $RMSE_{cv}$ of 3.53%. For its part, a $RMSE_{cv}$ of 3.33% was achieved for the Sentinel-2 parsimonious model trained with the five most informative bands (Fig. 4B). It should be noted that, from five bands onwards, no significant improvement in model accuracy was observed when keeping additional bands beyond

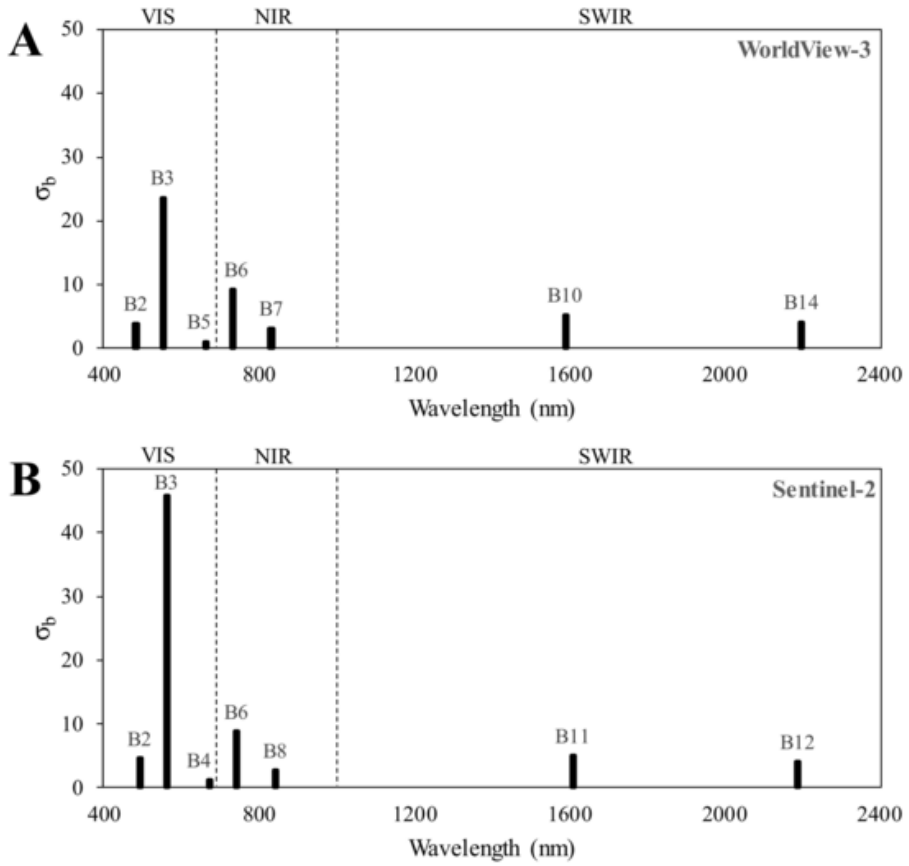

Fig. 4. WorldView-3 (A) and Sentinel-2 (B) band contribution to the 10-fold cross validated (CV) Gaussian processes regression (GPR) model of FVC trained with simulated reflectance data. Lower σ_b values correspond to higher predictive capacity of the band.

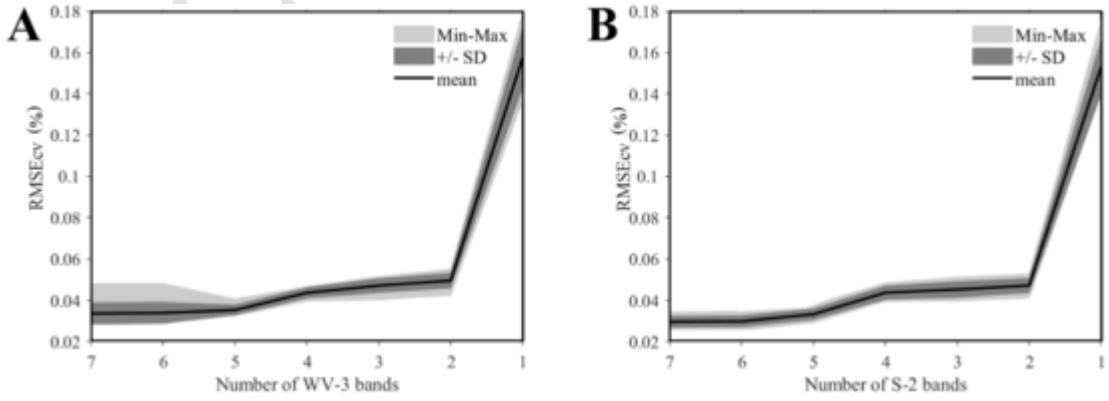

Fig. 5. 10-fold cross validation RMSEcv statistics (mean, standard deviation range and minimum-maximum range) of the Gaussian processes regression (GPR) models trained with WorldView-3 (A) and Sentinel-2 (B) simulated reflectance in a sequential backward band removal procedure based on GPR model hyperparameter σ_b.

the parsimonious FVC models or it even decreased the model stability (Fig. 5), as well as the computational efficiency.

The accuracy of the GPR models trained with PROSAIL-D reflectance simulations used to retrieve FVC from WorldView-3 imagery with regard to the FVC field measurements (Fig. 6; R^2 = 0.73–0.89 and RMSE = 6.44% - 9.32%) was substantially higher than that achieved from Sentinel-2 (Fig. 7; R^2 = 0.63–0.82 and RMSE = 10.61% - 13.26%). Likewise, the parsimonious GPR models outperformed the full models for both sensors (Fig. 6 and Fig. 7). The performance of the parsimonious GPR models for FVC retrieval at landscape level was R^2 = 0.83 and RMSE = 7.92% for WorldView-3 (Fig. 6A) and R^2 = 0.73 and RMSE = 11.89% for Sentinel-2 (Fig. 7A). At the plant community level, FVC retrieval was more accurate for oak tree forests (Figs. 6D and 7D; RMSE = 6.44% - 11.91%) than for heathlands (Figs. 6B and 7B; RMSE = 7.68% - 13.26%) and broomlands (Figs. 6C and 7C; RMSE = 9.29% - 12.68%). FVC was slightly underestimated for almost the entire range of field sampled vegetation cover in all communities, as it can be observed from the 1:1-line and the fitted line of Sentinel-2 FVC retrieval (Figs. 7B, C and D). For its part, at very low vegetation cover in shrub ecosystems, FVC retrieved from Sentinel-2 reflectance was slightly overestimated (Figs. 7B and C). These effects were much less noticeable or negligible in the FVC retrieval from WorldView-3 imagery (Fig. 6).

Based on WorldView-3 and Sentinel-2 parsimonious GPR models, we generated a map showing mean FVC predictions and their associated uncertainty (see Fig. 8 for a subset of the study area with a heterogeneous ground cover). It should be noted that even in bare soil or sparsely vegetated areas, the retrieval FVC uncertainty expressed as standard deviation around the mean GPR prediction is much lower in the WorldView-3 FVC map (Fig. 8B.1 and B.2) than for the Sentinel-2 FVC map (Fig. 8C.1 and C.2).

4. Discussion

The quantitative characterization of post-fire vegetation patterns in burned landscapes through remote sensing-based estimates of FVC is an essential approach to assess fire effects at different spatial scales and identify the post-fire recovery dynamic of vegetation communities (Zhang et al., 2013; Chu et al., 2016; Yang et al., 2017b; Fernández-Guisuraga et al., 2019a; Fernández-Guisuraga et al., 2020). This study is pioneer in the use of high spatial resolution satellite reflectance data to retrieve FVC by means of the GPR algorithm trained with RTM simulations, achieving promising results both at landscape and plant community levels. In contrast to empirical or pixel unmixing models, the hybrid RTM retrieval method can be applied to remote sensing scenes acquired over other burned landscapes with similar environmental characteristics to retrieve FVC without the need to use extensive field data to train the MLRA (Darvishzadeh et al., 2008). Only some field measurements would be required to validate the model (Liang et al., 2015) since it was parametrized without site-specific prior information that is not usually available at short or medium-term after fire. Although the use of site-specific prior information for leaf and canopy RTM parametrization may provide more realistic simulated spectra and alleviate the ill-posed nature of the model inversion (Yebra and Chuvieco, 2009; Verger et al., 2011; Jurdao et al., 2013), considerable accurate FVC estimations can still be achieved using a generic training simulation dataset as demonstrated in this study, among others (e.g. Baret et al., 2007; Qu et al., 2008; Verger et al., 2011; Liang et al., 2015; Jia et al., 2016; Campos-Taberner et al., 2018; García-Haro et al., 2018; Wang et al., 2018).

Regarding our first research question, FVC retrieval from GPR models trained with PROSAIL-D simulations based on WorldView-3 reflectance imagery outperformed the retrieval from Sentinel-2 imagery, both at landscape and community levels. This result indicates that the pixel size of WorldView-3 (2 m) is more appropriate to capture the fine scale of variation of the vegetation horizontal structure in the study site than that of Sentinel-2 (20 m). In fact, the main errors in the estimation of FVC are introduced by current retrieval algorithms when a coarse pixel encompasses a mixture of several ground vegetation and soil types in heterogeneous surfaces (Jurdao et al., 2013; Casas et al., 2014; Hu et al., 2020; Xu et al., 2020). These cover aggregation effect of mixed pixels produced a noticeable underestimation of retrieved FVC values from Sentinel-2 reflectance data for almost the entire range of field sampled vegetation, since coarse pixels produce average FVC values of a broader area than the ground scale of variation, being lower these averaged pixel values than fine-scale pixels (Fernández-Guisuraga et al., 2020; Kimm et al., 2020). By contrast, at low vegetation cover in shrub ecosystems, FVC was overestimated from Sentinel-2 reflectance data. According to Verrelst et al. (2015a), this behavior occurred due to a mismatch in the soil spectra profile acquired from expected pure bare soil pixels of Sentinel-2 imagery. Both under- and overestimation effects were much less noticeable in FVC retrieved from WorldView-3 reflectance data since (i) the land cover aggregation effect is not expected to occur at very high spatial resolution pixel size given the ground scale of variation of the ecosystems of our study area, and (ii) the acquisition of spectra profiles from very high spatial resolution of pure bare soil pixels of each soil type is obviously more precise (Fernández-Guisuraga et al., 2020).

FVC retrieval was improved from the GPR model training with only the most informative PROSAIL-D simulated reflectance data for WorldView-3 and Sentinel-2 matching bands (i.e. the parsimonious model for both sensors trained with blue and red bands, a band in the NIR region and the two SWIR bands). Some other researchers (e.g., Schlerf and Atzberger, 2006; Botha et al., 2010; Verrelst et al., 2016; Lunagaria and Patel, 2018) also reported that a spectral subsetting based on the selection of the most informative wavelengths improved the model retrieval accuracy by preventing model uncertainty which would bias the vegetation biophysical parameter retrieval (Meroni et al., 2004; Schlerf and Atzberger, 2006; Verrelst et al., 2016).

The higher accuracy of the retrieved FVC from both WorldView-3 and Sentinel-2 reflectance data in oak forests with respect to heathlands and broomlands could be explained by the complexity of biophysical parameters retrieval in shrublands. In such plant communities, a higher amount of non-photosynthetic material is exposed to the sensor compared to forest ecosystems (Casas et al., 2014). Indeed, even in a high resolution WorldView-3 pixel, a mixture of different shrub species can occur, although to a lesser extent than in a Sentinel-2 pixel (Fernández-Guisuraga et al., 2020). Another factor of uncertainty was related to model inversion being performed on simulated data using a turbid medium RTM as boundary condition (Verrelst et al., 2015a). A higher accuracy in the inversion could be provided by using a geometric RTM to simulate reflectance data in heterogeneous shrub ecosystems (Yebra et al., 2008), but at the expense of a much higher computational demand and a more complex parameterization of the model (Darvishzadeh et al., 2008). However, the 4SAIL canopy RTM used in this study is numerically more robust and stable than previous SAIL models (Jacquemoud et al., 2006; Verhoef et al., 2007). First, 4SAIL can describe non-homogeneous canopy characteristics in sparsely vegetated areas, since it can simulate precisely multiple scattering for optical and thermal radiation inside the canopy (Verhoef et al., 2007; Liang et al., 2015; Cao et al., 2018). Second, the formulation of the analytical solution implemented in 4SAIL avoid the mathematical singularity problem present in previous SAIL models, caused by duplicate eigenvalues in the analytical solution by means of eigenvector decomposition, which could lead to model numerical instability (see Verhoef, 1998; Verhoef and Bach, 2007; and Verhoef et al., 2007 for more details). In response to our second research question, the extension of the simulated PROSAIL-D spectra with several soil types and charred woody debris spectra profiles to account for these representative land covers of a recently burned landscape led to a reasonable performance (R^2 > 0.7 and RMSE < 9.3%) of FVC retrieval from WorldView-3 reflectance data even in shrub communities.

The prediction error of the WorldView-3 FVC estimation is well below (RMSE between 6.44% - 9.32%) the accepted accuracy threshold of 10% for biophysical variable retrieval (Drusch et al., 2012; Verrelst et al., 2016). This result suggests that FVC retrieval over heterogeneous burned areas limits the application of remote sensing imagery with decametric resolution, requiring the use of very high spatial resolution reflectance data for this purpose (Tao et al., 2019; Hu et al., 2020). Indeed, the high resolution FVC map generated for a portion of the study area showed a large spatial variability in the ground patterns which

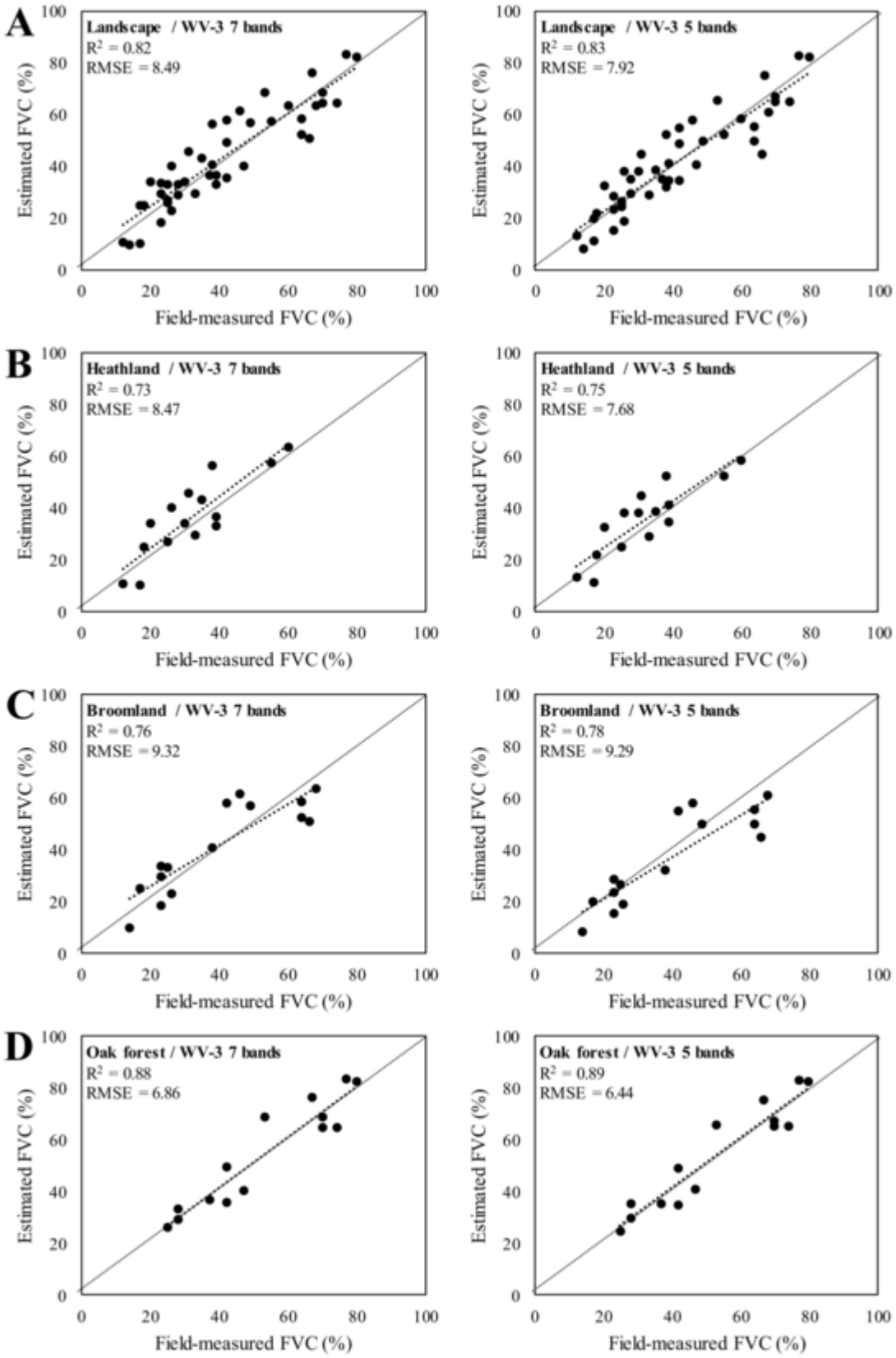

Fig. 6. Relationship between field-sampled and retrieved FVC from very high spatial resolution WorldView-3 (WV-3) imagery using the full (7 bands) and parsimonious (5 bands) Gaussian processes regression (GPR) models: landscape (A), heathlands (B), broomlands (C) and oak forests (D).

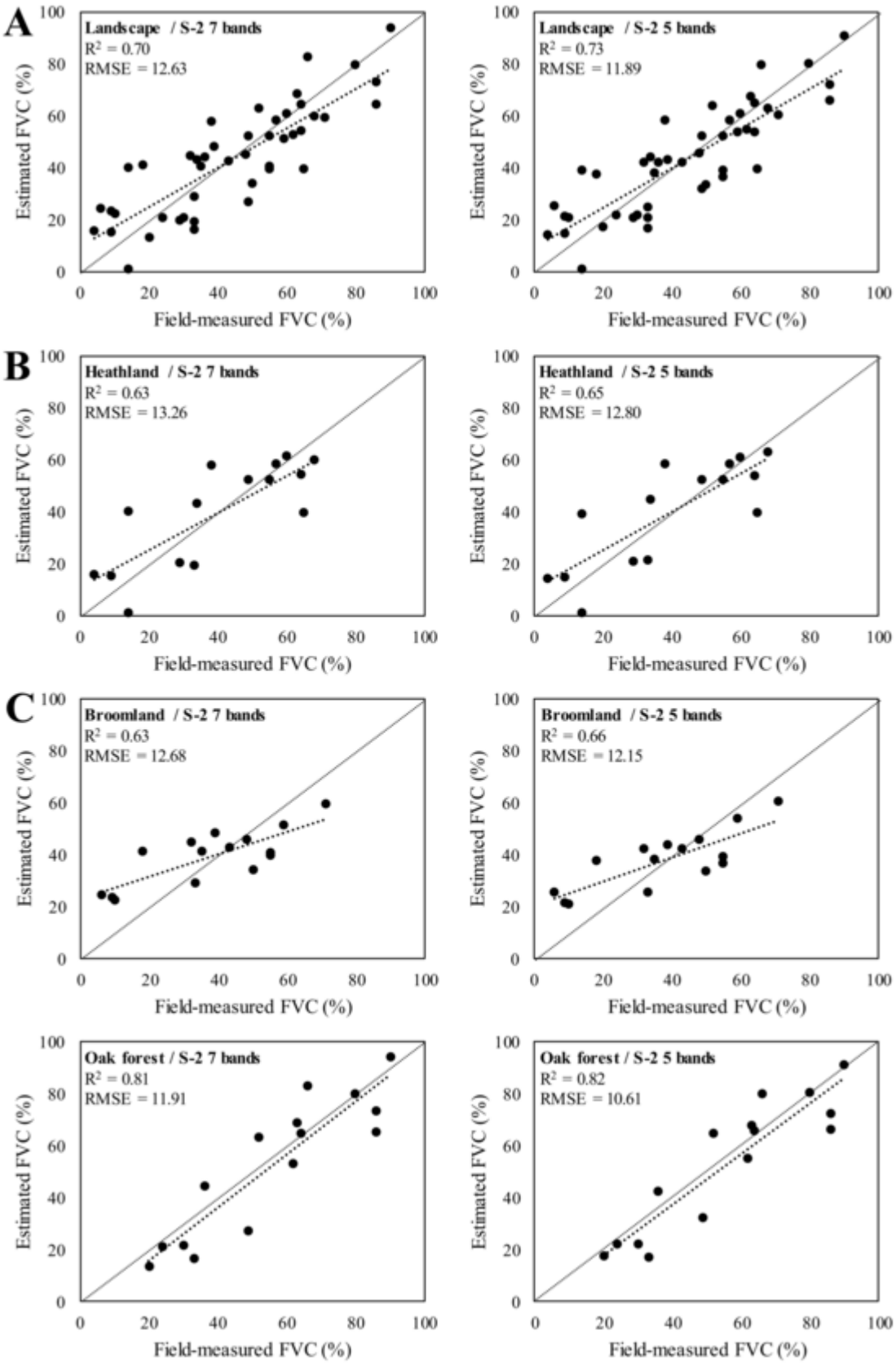

Fig. 7. Relationship between field-sampled and retrieved FVC from high spatial resolution Sentinel-2 (S-2) imagery using the full (7 bands) and parsimonious (5 bands) Gaussian processes regression (GPR) models: landscape (A), heathlands (B), broomlands (C) and oak forests (D).

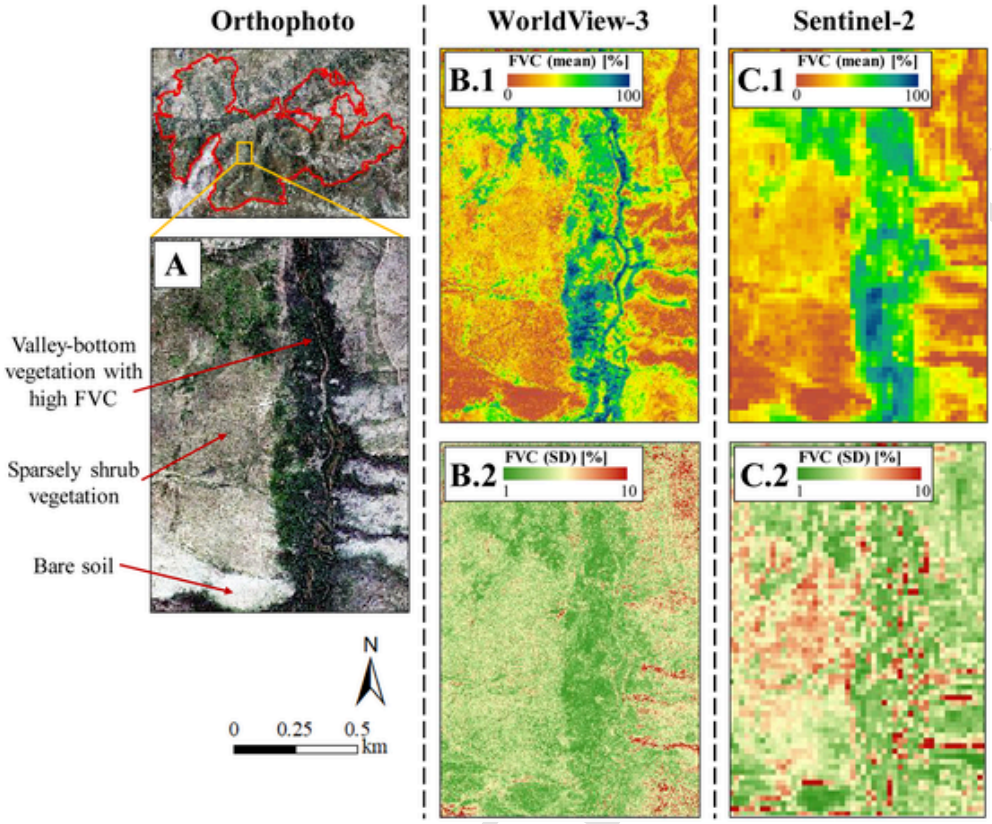

Fig. 8. Orthophoto at a spatial resolution of 0.5 m for a portion of the study area with heterogeneous ground cover (A) and mean predicted FVC maps and their associated uncertainty (standard deviation; SD) generated from the WorldView-3 (B.1 and B.2) and Sentinel-2 (C.1 and C.2) parsimonious Gaussian processes regression (GPR) model, at a spatial resolution of 2 m and 20 m, respectively. See Figure SM3 of the Supplementary material for a FVC map of the entire fire perimeter.

thanks to Bayesian probabilistic approach of the GPR model (Verrelst et al., 2015a) only remains at acceptable levels in the WorldView-3 FVC map. In addition, the lower revisit time of WorldView-3 satellite (< 1 day), in comparison to the combined Sentinel-2 constellation (5 days), provides a benefit for the assessment of vegetation condition at short-term after fire. In fact, emergency post-fire management actions should be implemented as soon as possible after disturbances, particularly in areas where the loss of vegetation exposes soil to erosion (USDA, 2020).

Despite the promising findings reported in this research, several limitations should be highlighted: (i) Although we considered equivalent bands to retrieve FVC from WorldView-3 and Sentinel-2 reflectance data, differences in the spectral response functions between both sensors, and particularly in the central wavelength location and width of SWIR bands, could be a potential source of uncertainty in the observed reflectance as a function of the ground cover type (Trishchenko et al., 2002; Cundill et al., 2015; Roy et al., 2016), together with satellite imagery pre-processing, such as atmospheric correction (Yebra et al., 2008). (ii) Despite having been used successfully in recent remote sensing studies (e.g. Fernández-Guisuraga et al., 2020), FVC field measurements collected using a visual estimation method are a source of uncertainty that may affect the accuracy of the global approach. Even though the use of digital cameras is a common procedure to measure field FVC (Zhou and Robson, 2001; Wang and Qi, 2008; Delamater et al., 2012; Ding et al., 2016; Wang et al., 2018) and reduce the visual estimation method uncertainty, the measurement of canopy FVC in forest tree ecosystems from a bottom-up direction is affected by shielding of photosynthetic vegetation in the upper part of the canopy by non-photosynthetic vegetation (e.g. branches), the FVC being underestimated in these circumstances (Jia et al., 2016). Hence, the use of unmanned aerial vehicles to measure tree canopy FVC in a bottom-up direction from low altitude flights should be considered in future studies.

5. Conclusions

The quantification of vegetation structure through the estimation of biophysical properties in forest landscapes affected by fire is essential to determine the impact of this disturbance at different spatio-temporal scales. This is a pioneer multi-scale study evaluating the potential of a radiative transfer model (RTM) inversion approach for estimating fractional vegetation cover (FVC) from satellite reflectance data at high spatial resolution, in comparison to the standard use of coarser imagery, both at landscape and community levels. FVC retrieval from WorldView-3 imagery at 2 m of spatial resolution outperforms the retrieval from Sentinel-2 imagery at 20 m, at both ecological levels, using Gaussian processes regression (GPR) models trained with PROSAIL-D simulations. WorldView-3 FVC retrieval shows negligible bias by avoiding the land cover aggregation effect of mixed pixels that encompass several vegetation and soil types and by the acquisition of more pure soil spectra profiles. These findings emphasize the use of high spatial resolution reflectance data for retrieving FVC over heterogeneous burned landscapes in order to capture the large ground spatial variability and reduce the associated uncertainty of FVC predictions in these sites. Finally, the hybrid RTM retrieval method used in this study is computationally efficient and does not require site-specific prior information that is not usually available at short or medium-term after fire, so this approach is proposed as a valuable tool for supporting post-fire management strategies.

Uncited references

García-Llamas et al., 2020

CRediT authorship contribution statement

José Manuel Fernández-Guisuraga: Conceptualization, Methodology, Validation, Formal analysis, Investigation, Writing - original draft. **Jochem Verrelst:** Methodology, Software, Writing - review & editing. **Leonor Calvo:** Conceptualization, Methodology, Investigation, Resources, Writing - review & editing, Project administration, Funding acquisi-

tion. **Susana Suárez-Seoane:** Conceptualization, Methodology, Investigation, Resources, Writing - review & editing, Project administration, Funding acquisition.

Declaration of Competing Interest

None.

Acknowledgements

This study was financially supported by the Spanish Ministry of Economy and Competitiveness, and the European Regional Development Fund (ERDF), in the framework of the GESFIRE (AGL2013-48189-C2-1-R) and FIRESEVES (AGL2017-86075-C2-1-R) projects; and by the Regional Government of Castilla and León in the framework of the FIRECYL (LE033U14) and SEFIRECYL (LE001P17) projects. J.M. Fernández-Guisuraga is supported by a predoctoral fellowship from the Spanish Ministry of Education (FPU16/03070). J. Verrelst is supported by the European Research Council (ERC) under the ERC-2017-STG SENTIFLEX project (755617).

Appendix A. Supplementary data

Supplementary data to this article can be found online at https://doi.org/10.1016/j.rse.2021.112304.

References

Anderson, S., Anderson, W., Hines, F., Fountain, A., 2005. Determination of field sampling methods for the assessment of curing levels in grasslands. Bushfire Cooperative Research Centre. In: Project A1.4 Report.

Archibald, S., Lehmann, C.E.R., Belcher, C.M., Bond, W.J., Bradstock, R.A., Daniau, A.L., Dexter, K.G., Forrestel, E.J., Greve, M., He, T., Higgins, S.I., Hoffmann, W.A., Lamont, B.B., McGlinn, D.J., Moncrieff, G.R., Osborne, C.P., Pausas, J.G., Price, O., Ripley, B.S., Rogers, B.M., Schwilk, D.W., Simon, M.F., Turetsky, M.R., Van der Werf, G.R., Zanne, A.E., 2018. Biological and geophysical feedbacks with fire in the earth system. Environ. Res. Lett. 13, 033003.

Asadzadeh, S., de Souza-Filho, C.R., 2016. Investigating the capability of WorldView-3 superspectral data for direct hydrocarbon detection. Remote Sens. Environ. 173, 162–173.

Bacour, C., Baret, F., Béal, D., Weiss, M., Pavageau, K., 2006. Neural network estimation of LAI, fAPAR, fCover and LAI×cab, from top of canopy MERIS reflectance data: principles and validation. Remote Sens. Environ. 105, 313–325.

Baret, F., Hagolle, O., Geiger, B., Bicheron, P., Miras, B., Huc, M., Berthelot, B., Niño, F., Weiss, M., Samain, O., Roujean, J.L., Leroy, M., 2007. LAI, fAPAR and fCover CYCLOPES global products derived from VEGETATION: part 1: principles of the algorithm. Remote Sens. Environ. 110, 275–286.

Bennett, L.T., Bruce, M.J., MacHunter, J., Kohout, M., Tanase, M.A., Aponte, C., 2016. Mortality and recruitment of fire-tolerant eucalypts as influenced by wildfire severity and recent prescribed fire. For. Ecol. Manag. 380, 107–117.

Bian, J., Li, A., Zhang, Z., Zhao, W., Lei, G., Xia, H., Tan, J., 2016. Grassland fractional vegetation cover monitoring using the composited HJ-1A/B time series images and unmanned aerial vehicles: a case study in Zoige wetland, China. Proceedings of the IEEE International Geoscience and Remote Sensing Symposium 7192–7195.

Botha, E.J., Leblon, B., Zebarth, B.J., Watmough, J., 2010. Non-destructive estimation of wheat leaf chlorophyll content from hyperspectral measurements through analytical model inversion. Int. J. Remote Sens. 31, 1679–1697.

Calvo, L., Santalla, S., Valbuena, L., Marcos, E., Tárrega, R., Luis-Calabuig, E., 2008. Post-fire natural regeneration of a Pinus pinaster forest in NW Spain. Plant Ecol. 197, 81–90.

Campos-Taberner, M., García-Haro, F.J., Camps-Valls, G., Grau-Muedra, G., Nutini, F., Crema, A., Boschetti, M., 2016. Multitemporal and multiresolution leaf area index retrieval for operational local rice crop monitoring. Remote Sens. Environ. 187, 102–118.

Campos-Taberner, M., Moreno-Martínez, Á., García-Haro, F.J., Camps-Valls, G., Robinson, N.P., Kattge, J., Running, S.W., 2018. Global estimation of biophysical variables from google earth engine platform. Remote Sens. 10, 1167.

Cao, B., Guo, M., Fan, W., Xu, X., Peng, J., Ren, H., Du, Y., Li, H., Bian, Z., Hu, T., Xiao, Q., Liu, Q., 2018. A new directional canopy emissivity model based on spectral invariants. IEEE Trans. Geosci. Remote Sens. 56, 6911–6926.

Casas, A., Riaño, D., Ustin, S.L., Dennison, P., Salas, J., 2014. Estimation of water-related biochemical and biophysical vegetation properties using multitemporal airborne hyperspectral data and its comparison to MODIS spectral response. Remote Sens. Environ. 148, 28–41.

Chergui, B., Fahd, S., Santos, X., Pausas, J.G., 2018. Socioeconomic factors drive fire-regime variability in the Mediterranean Basin. Ecosystems 21, 619–628.

Chu, T., Guo, X., Takeda, K., 2016. Remote sensing approach to detect post-fire vegetation regrowth in Siberian boreal larch forest. Ecol. Indic. 62, 32–46.

Chuvieco, E., Kasischke, E.S., 2007. Remote sensing information for fire management and fire effects assessment. J. Geophys. Res. 112, G01S90.

Collins, L., Griffioen, P., Newell, G., Mellor, A., 2018. The utility of random forests for

Corona, P., Lamonaca, A., Chirici, G., 2008. Remote sensing support for post fire forest management. iForest - biogeosciences and. Forestry 1, 6–12.

Cuevas-González, M., Gerard, F., Baltzer, H., Riaño, D., 2009. Analysing forest recovery after wildfire disturbance in boreal Siberia using remotely sensed vegetation indices. Glob. Chang. Biol. 15, 561–577.

Cundill, S.L., Van der Werff, H.M.A., Van der Meijde, M., 2015. Adjusting spectral indices for spectral response function differences of very high spatial resolution sensors simulated from field spectra. Sensors 15, 6221–6240.

Danner, M., Berger, K., Wocher, M., Mauser, W., Hank, T., 2019. Fitted PROSAIL parameterization of leaf inclinations, water content and Brown pigment content for winter wheat and maize canopies. Remote Sens. 11, 1150.

Darvishzadeh, R., Skidmore, A., Schlerf, M., Atzberger, C., 2008. Inversion of a radiative transfer model for estimating vegetation LAI and chlorophyll in a heterogeneous grassland. Remote Sens. Environ. 112, 2592–2604.

De Santis, A., Chuvieco, 2007. Burn severity estimation from remotely sensed data: performance of simulation versus empirical models. Remote Sens. Environ. 108, 422–435.

De Santis, A., Chuvieco, E., Vaughan, P.J., 2009. Short-term assessment of burn severity using the inversion of PROSPECT and GeoSail models. Remote Sens. Environ. 113, 126–136.

Delamater, P.L., Messina, J.P., Mark, J.K., Cochrane, A., 2012. A hybrid visual estimation method for the collection of ground truth fractional coverage data in a humid tropical environment. Int. J. Appl. Earth Obs. Geoinf. 18, 504–514.

DigitalGlobe WorldView-3 Datasheethttps://dg-cms-uploads-production.s3.amazonaws.com/uploads/document/file/95/DG2017_WorldView-3_DS.pdf2020(accessed 05 May 2020)

Ding, Y., Zhang, H., Li, Z., Xin, X., Zheng, X., Zhao, K., 2016. Comparison of fractional vegetation cover estimations using dimidiate pixel models and look-up table inversions of the PROSAIL model from Landsat 8 OLI data. J. Appl. Remote. Sens. 10, 036022.

Drusch, M., Del Bello, U., Carlier, S., Colin, O., Fernandez, V., Gascon, F., Hoersch, F., Isola, C., Laberinti, P., Martimort, P., Meygret, A., Spoto, F., Sy, O., Marchese, F., Bargellini, P., 2012. Sentinel-2: ESA's optical high-resolution mission for GMES operational services. Remote Sens. Environ. 120, 25–36.

ESA Sentinel-2 User Guidehttps://sentinel.esa.int/web/sentinel/user-guides/sentinel-2-msi2020(accessed 05 May 2020)

Fang, H., Li, W., Myneni, R.B., 2013. The impact of potential land cover misclassification on MODIS leaf area index (LAI) estimation: a statistical perspective. Remote Sens. 5, 830–844.

Féret, J.B., Gitelson, A.A., Noble, S.D., Jacquemoud, S., 2017. PROSPECT-D: towards modeling leaf optical properties through a complete lifecycle. Remote Sens. Environ. 193, 204–215.

Fernandes, P.M., Vega, J.A., Jiménez, E., Rigolot, E., 2008. Fire resistance of European pines. For. Ecol. Manag. 256, 246–255.

Fernández-Guisuraga, J.M., Suárez-Seoane, S., Calvo, L., 2019a. Modeling Pinus pinaster forest structure after a large wildfire using remote sensing data at high spatial resolution. For. Ecol. Manag. 446, 257–271.

Fernández-Guisuraga, J.M., Calvo, L., Fernández-García, V., Marcos-Porras, E., Taboada, A., Suárez-Seoane, S., 2019b. Efficiency of remote sensing tools for post-fire management along a climatic gradient. For. Ecol. Manag. 433, 553–562.

Fernández-Guisuraga, J.M., Calvo, L., Suárez-Seoane, S., 2020. Comparison of pixel unmixing models in the evaluation of post-fire forest resilience based on temporal series of satellite imagery at moderate and very high spatial resolution. ISPRS J. Photogramm. Remote Sens. 164, 217–228.

García-Haro, F.J., Campos-Taberner, M., Muñoz-Marí, J., Laparra, V., Camacho, F., Sánchez-Zapero, J., Camps-Valls, G., 2018. Derivation of global vegetation biophysical parameters from EUMETSAT Polar System. ISPRS J. Photogramm. Remote Sens. 139, 57–74.

García-Llamas, P., Suárez-Seoane, S., Fernández-Guisuraga, J.M., Fernández-García, V., Fernández-Manso, A., Quintano, C., Taboada, A., Marcos, E., Calvo, L., 2019. Evaluation and comparison of Landsat 8, Sentinel-2 and Deimos-1 remote sensing indices for assessing burn severity in Mediterranean fire-prone ecosystems. Int. J. Appl. Earth Obs. Geoinf. 80, 137–144.

García-Llamas, P., Suárez-Seoane, S., Fernández-Manso, A., Quintano, C., Calvo, L., 2020. Evaluation of fire severity in fire prone-ecosystems of Spain under two different environmental conditions. J. Environ. Manag. 271, 110706.

Gastellu-Etchegorry, J.P., Martin, E., Gascon, F., 2004. DART: a 3D model for simulating satellite images and studying surface radiation budget. Int. J. Remote Sens. 25, 73–96.

GEODE Mapa Geológico Digital continuo de Españahttp://mapas.igme.es/gis/services/Cartografia_Geologica/IGME_Geode_50/MapServer/WMSServer/2019(accessed 05 May 2020)

Gitelson, A.A., Kaufman, Y.J., Stark, R., Rundquist, D., 2002. Novel algorithms for remote estimation of vegetation fraction. Remote Sens. Environ. 80, 76–87.

Goetz, S.J., Fiske, G.J., Bunn, A.G., 2006. Using satellite time-series data sets to analyze fire disturbance and forest recovery across Canada. Remote Sens. Environ. 101, 352–365.

González-De Vega, S., De las Heras, J., Moya, D., 2016. Resilience of Mediterranean terrestrial ecosystems and fire severity in semiarid areas: responses of Aleppo pine forests in the short, mid and long term. Sci. Total Environ. 573, 1171–1177.

Gould, K.S., 2004. Nature's swiss army knife: the diverse protective roles of anthocyanins in leaves. J. Biomed. Biotechnol. 5, 314–320.

Gutman, G., Ignatov, A., 1998. The derivation of the green vegetation fraction from NOAA/AVHRR data for use in numerical weather prediction models. Int. J. Remote Sens. 19, 1533–1543.

Hill, M.J., Zhou, Q., Sun, Q., Schaaf, C.B., Palace, M., 2017. Relationships between vegetation indices, fractional cover retrievals and the structure and composition of Brazilian Cerrado natural vegetation. Int. J. Remote Sens. 38, 874–905.

Houborg, R., McCabe, M.F., 2018. A hybrid training approach for leaf area index estimation via cubist and random forests machine-learning. ISPRS J. Photogramm. Remote Sens. 135, 173–188.

Hu, Q., Yang, J., Xu, B., Huang, J., Memon, M.S., Yin, G., Zeng, Y., Zhao, J., Liu, K., 2020. Evaluation of global decametric-resolution LAI, FAPAR and FVC estimates derived

Jacquemoud, S., Baret, F., 1990. PROSPECT: a model of leaf optical properties spectra. Remote Sens. Environ. 34, 75–91.
Jacquemoud, S., Verhoef, W., Baret, F., Zarco-Tejada, P., Asner, G., Francois, C., Ustin, S., 2006. PROSPECT + SAIL: 15 Years of Use for Land Surface Characterization. 2006 IEEE International Symposium on Geoscience and Remote Sensing. Denver, United States.
Jacquemoud, S., Verhoef, W., Baret, F., Bacour, C., Zarco-Tejada, P.J., Asner, G.P., François, C., Ustin, S.L., 2009. PROSPECT + SAIL models: a review of use for vegetation characterization. Remote Sens. Environ. 113, 56–66.
Jay, S., Bendoula, R., Hadoux, X., Féret, J.B., Gorretta, N., 2016. A physically-based model for retrieving foliar biochemistry and leaf orientation using close-range imaging spectroscopy. Remote Sens. Environ. 177, 220–236.
Jia, K., Liang, S., Liu, S., Li, Y., Xiao, Z., Yao, Y., Jiang, B., Zhao, X., Wang, X., Xu, S., Cui, J., 2015. Global land surface fractional vegetation cover estimation using general regression neural networks from MODIS surface reflectance. IEEE Trans. Geosci. Remote Sens. 53, 4787–4796.
Jia, K., Liang, S., Gu, X., Baret, F., Wei, X., Wang, X., Yao, Y., Yang, L., Li, Y., 2016. Fractional vegetation cover estimation algorithm for Chinese GF-1 wide field view data. Remote Sens. Environ. 177, 184–191.
Jiapaer, G., Chen, X., Bao, A., 2011. A comparison of methods for estimating fractional vegetation cover in arid regions. Agric. For. Meteorol. 151, 1698–1710.
Jurdao, S., Yebra, M., Guerschman, J.P., Chuvieco, E., 2013. Regional estimation of woodland moisture content by inverting radiative transfer models. Remote Sens. Environ. 132, 59–70.
Kallel, A., Le Hégarat-Mascle, S., Ottlé, C., Hubert-Moy, L., 2007. Determination of vegetation cover fraction by inversion of a four-parameter model based on isoline parametrization. Remote Sens. Environ. 111, 553–566.
Kasischke, E.S., Stocks, B.J., 2000. Fire, climate change. In: And Carbon Cycling in the Boreal Forest. Springer-Verlag, New York.
Keeley, J.E., Zedler, P.H., 1998. Evolution of life histories in Pinus. In: Richardson, D.M. (Ed.), Ecology and Biogeography of Pinus. Cambridge University Press, Cambridge, pp. 219–250.
Kimm, H., Guan, K., Jiang, C., Peng, B., Gentry, L.F., Wilkin, S.C., Wang, S., Cai, Y., Bernacchi, C.J., Peng, J., Luo, Y., 2020. Deriving high-spatiotemporal-resolution leaf area index for agroecosystems in the U.S. Corn Belt using Planet Labs CubeSat and STAIR fusion data. Remote Sens. Environ. 239, 111615.
Kokaly, R.F., Rockwell, B.W., Haire, S.L., King, T.V.V., 2007. Characterization of post-fire surface cover, soils, and burn severity at the Cerro Grande fire, New Mexico, using hyperspectral and multispectral remote sensing. Remote Sens. Environ. 106, 305–325.
Lee, C., Schlemme, C., Murray, J., Unsworth, R., 2015. The cost of climate change: ecosystem services and wildland fires. Ecol. Econ. 116, 261–269.
Lentile, L.B., Holden, Z.A., Smith, A.M.S., Falkowski, M.J., Hudak, A.T., Morgan, P., Lewis, S.A., Gessler, P.E., Benson, N.C., 2006. Remote sensing techniques to assess active fire characteristics and post-fire effects. Int. J. Wildland Fire 15, 319–345.
Li, Y., Wang, H., Li, X.B., 2015a. Fractional vegetation cover estimation based on an improved selective endmember spectral mixture model. PLoS One 10 (4), e0124608.
Li, W., Weiss, M., Waldner, F., Defourny, P., Demarez, V., Morin, D., Hagolle, O., Baret, F., 2015b. A generic algorithm to estimate LAI, FAPAR and FCOVER variables from SPOT4_HRVIR and Landsat sensors: evaluation of the consistency and comparison with ground measurements. Remote Sens. 7, 15494–15516.
Liang, Z., Bing-fang, W., Yue-min, Z., Ji-hua, M., Ning, Z., 2008. A study of fast estimation of vegetation fraction in three gorges emigration area by using SPOT5 imagery. Int. Arch. Photogramm. Remote. Sens. Spat. Inf. Sci. 37, 987–992.
Liang, S., Li, X., Wang, J., 2012. Advanced Remote Sensing: Terrestrial Information Extraction and Applications. Academic Press, Cambridge, United States.
Liang, L., Di, L., Zhang, L., Deng, M., Qin, Z., Zhao, S., Lin, H., 2015. Estimation of crop LAI using hyperspectral vegetation indices and a hybrid inversion method. Remote Sens. Environ. 165, 123–134.
Lin, J., Pan, Y., Lyu, H., Zhu, X., Li, X., Dong, B., Li, H., 2019. Developing a two-step algorithm to estimate the leaf area index of forests with complex structures based on CHRIS/PROBA data. For. Ecol. Manag. 441, 57–70.
Liu, H., Randerson, J.T., Lindfors, J., Chapin III, F. S., 2005. Changes in the surface energy budget after fire in boreal ecosystems of interior Alaska: an annual perspective, J. Geophys. Res., 110: D13101.
Liu, Z., Ballantyne, A.P., Cooper, L.A., 2018. Increases in land surface temperature in response to fire in Siberian boreal forests and their attribution to biophysical processes. Geophys. Res. Lett. 45, 6485–6494.
Los, S.O., Collatz, G.J., Sellers, P.J., Malmström, C.M., Pollack, N.H., DeFries, R.S., Bounoua, L., Parris, M.T., Tucker, C.J., Dazlich, D.A., 2000. A global 9-year biophysical land-surface data set from NOAA AVHRR data. J. Hydrometeorol. 1, 183–199.
Lozano, F.J., Suárez-Seoane, S., Kelly, M., Luis-Calabuig, E., 2008. A multi-scale approach for modeling fire occurrence probability using satellite data and classification trees: a case study in a mountainous Mediterranean region. Remote Sens. Environ. 112, 708–719.
Ludwig, J.A., Wilcox, B.P., Breshears, D.D., Tongway, D.J., Imeson, A.C., 2005. Vegetation patches and runoff–erosion as interacting ecohydrological processes in semiarid landscapes. Ecology 86, 288–297.
Lunagaria, M.M., Patel, H.R., 2018. Evaluation of PROSAIL inversion for retrieval of chlorophyll, leaf dry matter, leaf angle, and leaf area index of wheat using spectrodirectional measurements. Int. J. Remote Sens. 40, 8125–8145.
McKay, M.D., Beckman, R.J., Conover, W.J., 1979. A comparison of three methods for selecting values of input variables in the analysis of output from a computer code. Technometrics 21, 239–245.
Meroni, M., Colombo, R., Panigada, C., 2004. Inversion of a radiative transfer model with hyperspectral observations for LAI mapping in poplar plantations. Remote Sens. Environ. 92, 195–206.
Mu, X., Huang, S., Ren, H., Yan, G., Song, W., Ruan, G., 2015. Validating GEOV1 fractional vegetation cover derived from coarse-resolution remote sensing images over croplands. IEEE J. Selected Topics Appl. Earth Observ. Remote Sens. 8, 439–446.
Nilson, T.A., 1971. Theoretical analysis of the frequency of gaps in plant stands. Agric. Meteorol. 8, 25–38.
Ninyerola, M., Pons, X., Roure, J.M., 2005. Atlas Climático Digital de la Península Ibérica. Metodología y aplicaciones en bioclimatología y geobotánica. Universidad Autónoma de Barcelona.
Pausas, J.G., Keeley, J.E., 2014. Abrupt climate-independent fire regime changes. Ecosystems 17, 1109–1120.
Pausas, J.G., Llovet, J., Rodrigo, A., Vallejo, R., 2008. Are wildfires a disaster in the Mediterranean basin? A review. Int. J. Wildland Fire 17, 713–723.
Puigdefábregas, J., 2005. The role of vegetation patterns in structuring runoff and sediment fluxes in drylands. Earth Surf. Process. Landf. 30, 133–147.
Qu, Y., Wang, J., Wan, H., Li, X., Zhou, G., 2008. A Bayesian network algorithm for retrieving the characterization of land surface vegetation. Remote Sens. Environ. 112, 613–622.
Quayle, B., Brewer, K., Williams, K., 2005. Monitoring post-fire vegetation recovery of wildland fire areas in the western united states using MODIS data. In: Pecora 16: Global Priorities in Land Remote Sensing, Sioux Falls, United States.
Rasmussen, C.E., Williams, C.K.I., 2006. Gaussian Processes for Machine Learning. The MIT Press, New York.
Richter, R., Schläpfer, D., 2018. Atmospheric / topographic correction for satellite imagery. In: DLR Report DLR-IB 565–01/2018, Wessling, Germany.
Rivas-Martínez, S., Rivas-Sáenz, S., Penas, A., 2011. Worldwide bioclimatic classification system. Global Geobotany. In: 1: 1–634 + 4 Maps.
Rivera, J.P., Verrelst, J., Leonenko, G., Moreno, J., 2013. Multiple cost functions and regularization options for improved retrieval of leaf chlorophyll content and LAI through inversion of the PROSAIL model. Remote Sens. 5, 3280–3304.
Robinne, F.N., Hallema, D.W., Bladon, K.D., Buttle, J.M., 2020. Wildfire impacts on hydrologic ecosystem services in north American high-latitude forests: a scoping review. J. Hydrol. 581, 124360.
Roy, D.P., Kovalskyy, V., Zhang, H.K., Vermote, E.F., Yan, L., Kumar, S.S., Egorov, A., 2016. Characterization of Landsat-7 to Landsat-8 reflective wavelength and normalized difference vegetation index continuity. Remote Sens. Environ. 185, 57–70.
Schlawin, J.R., Zahawi, R.A., 2008. "Nucleating" succession in recovering neotropical wet forests: the legacy of remnant trees. J. Veg. Sci. 19, 485–492.
Schlerf, M., Atzberger, C., 2006. Inversion of a forest reflectance model to estimate biophysical canopy variables from hyperspectral remote sensing data. Remote Sens. Environ. 100, 281–294.
Sinha, S.K., Padalia, H., Dasgupta, A., Verrelst, J., Rivera, J.P., 2020. Estimation of leaf area index using PROSAIL based LUT inversion, MLRA-GPR and empirical models: case study of tropical deciduous forest plantation, North India. Int. J. Appl. Earth Obs. Geoinf. 86 (102027).
Song, W., Mu, X., Ruan, G., Gao, Z., Li, L., Yan, G., 2017. Estimating fractional vegetation cover and the vegetation index of bare soil and highly dense vegetation with a physically based method. Int. J. Appl. Earth Obs. Geoinf. 58, 168–176.
Storey, E.A., Stow, D.A., O'Leary, J.F., 2016. Assessing postfire recovery of chamise chaparral using multi-temporal spectral vegetation index trajectories derived from Landsat imagery. Remote Sens. Environ. 183, 53–64.
Suchar, V.A., Crookston, N.L., 2010. Understory cover and biomass indices predictions for forest ecosystems of the Northwestern United States. Ecol. Indic. 10, 602–609.
Tao, G., Jia, K., Zhao, X., Wei, X., Xie, X., Zhang, X., Wang, B., Yao, Y., Zhang, X., 2019. Generating high Spatio-temporal resolution fractional vegetation cover by fusing GF-1 WFV and MODIS data. Remote Sens. 11, 2324.
Trishchenko, A.P., Cihlar, J., Li, Z., 2002. Effects of spectral response function on surface reflectance and NDVI measured with moderate resolution satellite sensors. Remote Sens. Environ. 81, 1–18.
Upreti, D., Huang, W., Kong, W., Pascucci, S., Pignatti, S., Zhou, X., Ye, H., Casa, R., 2019. A comparison of hybrid machine learning algorithms for the retrieval of wheat biophysical variables from Sentinel-2. Remote Sens. 11, 481.
USDA Burned Area Emergency Response - BAERhttps://www.fs.fed.us/naturalresources/watershed/burnedareas.shtml2020(accessed 06 November 2020)
Van Leeuwen, W.J.D., 2008. Monitoring the effects of Forest restoration treatments on post-fire vegetation recovery with MODIS multitemporal data. Sensors 8, 2017–2042.
Veraverbeke, S., Lhermitte, S., Verstraeten, W.W., Goossens, R., 2011. A time-integrated MODIS burn severity assessment using the multi-temporal differenced normalized burn ratio (dNBRMT). Int. J. Appl. Earth Obs. Geoinf. 13, 52–58.
Veraverbeke, S., Somers, B., Gitas, I., Katagis, T., Polychronaki, A., Goossens, R., 2012a. Spectral mixture analysis to assess post-fire vegetation regeneration using Landsat thematic mapper imagery: accounting for soil brightness variation. Int. J. Appl. Earth Obs. Geoinf. 14, 1–11.
Veraverbeke, S., Gitas, I., Katagis, T., Polychronaki, A., Somers, B., Goossens, R., 2012b. Assessing post-fire vegetation recovery using red–near infrared vegetation indices: accounting for background and vegetation variability. ISPRS J. Photogramm. Remote Sens. 68, 28–39.
Verger, A., Baret, F., Camacho, F., 2011. Optimal modalities for radiative transfer-neural network estimation of canopy biophysical characteristics: evaluation over an agricultural area with CHRIS/PROBA observations. Remote Sens. Environ. 115, 415–426.
Verhoef, W., 1984. Light scattering by leaf layers with application to canopy reflectance modeling: the SAIL model. Remote Sens. Environ. 16, 125–141.
Verhoef, W., 1985. Earth observation modeling based on layer scattering matrices. Remote Sens. Environ. 17, 165–178.
Verhoef, W., 1998. Theory of radiative transfer models applied in optical remote sensing of vegetation canopies PhD Thesis Wageningen Agricultural University, The Netherlands.
Verhoef, W., Bach, H., 2003. Simulation of hyperspectral and directional radiance images using coupled biophysical and atmospheric radiative transfer models. Remote Sens. Environ. 87, 23–41.
Verhoef, W., Bach, H., 2007. Coupled soil–leaf-canopy and atmosphere radiative transfer modeling to simulate hyperspectral multi-angular surface reflectance and TOA radiance data. Remote Sens. Environ. 109, 166–182.

Verhoef, W., Xiao, Q., Jia, L., Su, Z., 2007. Unified optical-thermal four-stream radiative transfer theory for homogeneous vegetation canopies. IEEE Trans. Geosci. Remote Sens. 45, 1808–1822.

Verrelst, J., Romijn, E., Kooistra, L., 2012a. Mapping vegetation structure in a heterogeneous river floodplain ecosystem using pointable CHRIS/PROBA data. Remote Sens. 4, 2866–2889.

Verrelst, J., Alonso, L., Camps-Valls, G., Delegido, J., Moreno, J., 2012b. Retrieval of vegetation biophysical parameters using Gaussian process techniques. IEEE Trans. Geosci. Remote Sens. 50, 1832–1843.

Verrelst, J., Muñoz, J., Alonso, L., Delegido, J., Rivera, J.P., Camps-Valls, G., Moreno, J., 2012c. Machine learning regression algorithms for biophysical parameter retrieval: opportunities for Sentinel-2 and -3. Remote Sens. Environ. 118, 127–139.

Verrelst, J., Rivera, J.P., Veroustraete, F., Muñoz-Marí, J., Clevers, J.G.P.W., Camps-Valls, G., Moreno, J., 2015a. Experimental Sentinel-2 LAI estimation using parametric, non-parametric and physical retrieval methods – a comparison. ISPRS J. Photogramm. Remote Sens. 108, 260–272.

Verrelst, J., Camps-Valls, G., Muñoz-Marí, J., Rivera, J.P., Veroustraete, F., Clevers, J.G.P.W., Moreno, J., 2015b. Optical remote sensing and the retrieval of terrestrial vegetation bio-geophysical properties – a review. ISPRS J. Photogramm. Remote Sens. 108, 273–290.

Verrelst, J., Rivera, J.P., Gitelson, A., Delegido, J., Moreno, J., Camps-Valls, G., 2016. Spectral band selection for vegetation properties retrieval using Gaussian processes regression. Int. J. Appl. Earth Obs. Geoinf. 52, 554–567.

Walker, R.B., Coop, J.D., Downing, W.M., Krawchuk, M.A., Malone, S.L., Meigs, G.W., 2019. How much forest persists through fire? High-resolution mapping of tree cover to characterize the abundance and spatial pattern of fire refugia across mosaics of burn severity. Forests 10, 782.

Wang, C., Qi, J., 2008. Biophysical estimation in tropical forests using JERS-1 SAR and VNIR imagery II. Aboveground woody biomass. Int. J. Remote Sens. 29, 6827–6849.

Wang, X., Jia, K., Liang, S., Li, Q., Wei, X., Yao, Y., Zhang, X., Tu, Y., 2017. Estimating fractional vegetation cover from Landsat-7 ETM + reflectance data based on a coupled radiative transfer and crop growth model. IEEE Trans. Geosci. Remote Sens. 55, 5539–5546.

Wang, B., Jia, K., Liang, S., Xie, X., Wei, X., Zhao, X., Yao, Y., Zhang, X., 2018. Assessment of Sentinel-2 MSI spectral band Reflectances for estimating fractional vegetation cover. Remote Sens. 10, 1927.

Weiss, M., Baret, F., Myneni, R.B., Pragnère, A., Knyazikhin, Y., 2000. Investigation of a model inversion technique to estimate canopy biophysical variables from spectral and directional reflectance data. Agronomie 20, 3–22.

White, M.A., Asner, G.P., Nemani, R.R., Privette, J.L., Running, S.W., 2000. Measuring fractional cover and leaf area index in arid ecosystems: digital camera, radiation transmittance, and laser altimetry methods. Remote Sens. Environ. 74, 45–57.

Wing, B.M., Ritchie, M.W., Boston, K., Cohen, W.B., Gitelman, A., Olsen, M.J., 2012. Prediction of understory vegetation cover with airborne lidar in an interior ponderosa pine forest. Remote Sens. Environ. 124, 730–741.

Xiao, J., Moody, A., 2005. A comparison of methods for estimating fractional green vegetation cover within a desert-to-upland transition zone in central New Mexico, USA. Remote Sens. Environ. 98, 237–250.

Xu, B., Li, J., Park, T., Liu, Q., Zeng, Y., Yin, G., Yan, K., Chen, C., Zhao, J., Fan, W., Knyazikhin, Y., Myneni, R.B., 2020. Improving leaf area index retrieval over heterogeneous surface mixed with water. Remote Sens. Environ. 240, 111700.

Yang, L., Jia, K., Liang, S., Liu, J., Wang, X., 2016. Comparison of four machine learning methods for generating the GLASS fractional vegetation cover product from MODIS data. Remote Sens. 8, 682.

Yang, L., Jia, K., Liang, S., Wei, X., Yao, Y., Zhang, X., 2017a. A robust algorithm for estimating surface fractional vegetation cover from Landsat data. Remote Sens. 9, 857.

Yang, J., Pan, S., Dangal, S., Zhang, B., Wang, S., Tian, H., 2017b. Continental-scale quantification of post-fire vegetation greenness recovery in temperate and boreal North America. Remote Sens. Environ. 199, 277–290.

Yebra, M., Chuvieco, E., 2009. Linking ecological information and radiative transfer models to estimate fuel moisture content in the Mediterranean region of Spain: solving the ill-posed inverse problem. Remote Sens. Environ. 113, 2403–2411.

Yebra, M., Chuvieco, E., Riaño, D., 2008. Estimation of live fuel moisture content from MODIS images for fire risk assessment. Agric. For. Meteorol. 148, 523–536.

Zhang, X., Liao, C., Li, J., Sun, Q., 2013. Fractional vegetation cover estimation in arid and semi-arid environments using HJ-1 satellite hyperspectral data. Int. J. Appl. Earth Obs. Geoinf. 21, 506–512.

Zhou, Q., Robson, M., 2001. Automated rangeland vegetation cover and density estimation using ground digital images and a spectral-contextual classifier. Int. J. Remote Sens. 22, 3457–3470.

Zhou, L., Dickinson, R.E., Tian, Y., Vose, R.S., Dai, Y., 2007. Impact of vegetation removal and soil aridation on diurnal temperature range in a semiarid region: application to the Sahel. PNAS 104, 17937–17942.